Newport Beach, CA, USA
ACTIVE 95
1995 July 06-08

CHARACTERIZATION OF TRANSFER FUNCTIONS FOR PIEZOCERAMIC AND CONVENTIONAL TRANSDUCERS

Bor-Tsuen Wang

Department of Mechanical Engineering
National Pingtung Polytechnic Institute
Pingtung, Taiwan 91207
Republic of China

ABSTRACT

This paper analytically derives the transfer functions for piezoceramic and conventional transducers and characterizes their relationships in terms of frequency response function (FRF) and modal parameters such as natural frequencies and mode shapes. A conventional approach for active structural vibration and sound radiation control may use point force shakers as actuators to suppress structural motion so as to reduce sound radiation from the structure. Accelerometers can then be attached to the structure serving as error sensors, while a proper control algorithm is implemented to perform active control. A newly developed piezoceramic transducers such as PZT and PVDF can be integrated into the structure and suitable for serving as actuators and sensors. This work is to determine the transfer functions between accelerometer/point force, accelerometer/PZT, PVDF/point force and PVDF/PZT. Their transfer functions are presented and characterized. The results show that those transfer functions are highly correlated. The mode shapes can also be properly identified. This work leads to a basis for active structural vibration and acoustic control and also draws an ideas for applications of smart structural testing to system identification and diagnosis.

INTRODUCTION

Piezoceramic transducers have been drawn many interests in the application of active structural vibration and acoustic control. The PZT (Lead-Zirconium-Titanate) ceramics are used for their ferroelectric properties, and usually applied as control actuators. The PZT dynamic actuation model for beam and plate structures have been developed (Dimitriadis et al., 1991; Crawley and de Luis, 1987; Wang and Rogers, 1991; Im and Atluri, 1989), and shown their validity for practical applications. The PVDF (polyfluoride) sheet which is a flexible film can be adhered to the structural surface serving as a sensor. A strip of PVDF film (Hubbard, 1987; Clark et al., 1991) or the shaped PVDF film (Lee and Moon, 1990) sensor has been developed and applied to structural vibration and acoustic control as well.

Alberts and Colvin (1991) derived the voltage transfer functions between PVDF actuation and sensing layers. They showed that the collocated actuator and sensor system is stable. Collin et al. (1991) compared the piezopolymer spatial filters with the conventional point sensor and

showed that the distributed sensor can improve the closed-loop performance of a control system. Sun et al. (1994) measured the electric admittance of PZT sensor/actuators so as to obtain mechanical frequency response function of a structure. The structural natural frequency, modal damping and curvature mode shapes can be properly extracted.

The FRF is so interested in control applications as well as for structural modal testing. This paper is to derive the transfer functions between piezoceramic transducers, such as PZT actuators and PVDF film sensors, and conventional transducers, such as point force actuators and accelerometers. The frequency response functions (FRFs) between accelerometer/point force, accelerometer/PZT actuator, PVDF sensor/point force, and PVDF sensor/PZT actuator are derived and expressed in modal model format. The individual mode shape of accelerometer, point force, PVDF film sensor or PZT actuator is identified and shown the orthogonality properties respectively. The orthogonal pair of mode shape leads to the physical interpolation of FRF and results in the theoretical feasibility of structural modal testing by using any combination of piezoceramic and conventional transducers. The point and transfer FRFs are numerically shown and demonstrated for their characteristics.

THEORETICAL ANALYSIS

Lateral Vibration of Uniform Beam. Consider a uniform simply-supported beam with length of L, as shown in Figure 1, the equation of motion can be obtained as follow:

$$E_b I\frac{\partial^4 w}{\partial x^4}+\rho_b b t_b\frac{\partial^2 w}{\partial t^2}=p(x,t) \tag{1}$$

where E_b is the Young's modulus of the beam; I the moment of inertia; ρ_b the beam density; t_b the beam thickness; b the beam width; $p(x,t)$ the force function. The boundary conditions for a simply-supported beam are

$$M(0,t)=M(L,t)=E_b I\frac{\partial^2 w}{\partial x^2}=0 \tag{2}$$

$$w(0,t)=w(L,t)=0 \tag{3}$$

For free vibration analysis, i.e., $p(x,t)=0$, the natural frequencies can be found to be

$$\omega_n=(n\pi)^2\sqrt{\frac{E_b I}{\rho_b b t_b L^4}} \tag{4}$$

The general form of beam lateral displacement, while the beam is subjected to harmonic inputs, can be written as the follow:

$$w(x,t)=e^{i\omega t}\sum_{n=1}^{\infty} W_n \sin\kappa_n x \tag{5}$$

where

$$\kappa_n=\frac{n\pi}{L} \tag{6}$$

$$W_n = \frac{P_n}{\rho_b b t_b (\omega_n^2 - \omega^2)} \tag{7}$$

Here ω is the excitation frequency; κ_n is the modal number; W_n is the modal amplitude; and P_n is the modal force depending on the forms of external forces. For a harmonic point force with the amplitude of F located at x_f acting on the beam, the force function, p(x,t), can be written as follow:

$$p(x,t) = F\delta(x - x_f)e^{i\omega t} \tag{8}$$

The Delta function, $\delta(x)$, is employed to represent the location of the point force. The modal force, P_n^f, due to the point force excitation is given as follow:

$$P_n^f = \frac{2F}{L}\sin\kappa_n x_f \tag{9}$$

where the superscript f signify the point force. For an actuator consisting of two identical piezoceramic patches bonded symmetrically on the two opposite beam surfaces and activated 180° out-of-phase, the equivalent external forces can be derived as follow (Wang and Rogers, 1991):

$$p(x,t) = K_c V_c[\delta'(x - x_1) - \delta'(x - x_2)]e^{i\omega t} \tag{10}$$

where K_c is some constant depending on physical properties of beam and PZT (Wang and Rogers, 1991; Crawley and de Luis, 1987); V_c is the applied voltage; and $K_c V_c$ is the concentrated moments acting on the both edges of piezoelectric patches represented by the first derivative of Delta function. The corresponding expression of modal force for PZT excitation, P_n^c, can be derived as follow:

$$P_n^c = K_c V_c \kappa_n \sin(\kappa_n l_c/2)\frac{2}{L}\sin\kappa_n x_c \tag{11}$$

where x_c and l_c are the central location and the length of the PZT actuator as shown in Figure 1.

PVDF Sensor's Equation. For a PVDF film arranged as shown in Figure 1, the shape function can be expressed as follow:

$$\Gamma(x) = u(x - x_p - l_p/2) - u(x - x_p + l_p/2) \tag{12}$$

where $u(x)$ is the step function; x_p and l_p are the central location and the length of the PVDF film respectively. The sensor's equation can then be derived as follows (Hubbard, 1987):

$$q(t) = \frac{t_b + t_p}{2} b_p e_{31} \int_0^L \Gamma(x)\frac{\partial^2 w}{\partial x^2} dx \tag{13}$$

$$V(t)=\frac{q(t)}{\epsilon A}t_p \tag{14}$$

where b_p is the sensor width; t_p the sensor thickness; e_{31} the piezoelectric field intensity constant; ϵ is the permittivity of PVDF films; A is the sensor area. By substituting $w(x,t)$ and integrating over the beam length, the generated voltages can then be expressed as:

$$V(t)=e^{i\omega t}\sum_{n=1}^{\infty} W_n K_p \kappa_n \sin(\kappa_n l_p/2)\sin\kappa_n x_p \tag{15}$$

K_p is some constant related to the physical properties of beam and PVDF. It is noted that the generated voltage is proportional to the slope difference between the two edges of a PVDF film (Hubbard, 1987).

Derivation of Frequency Response Functions. By harmonic analysis and employing the proportional damping model, the frequency response functions between each pair of accelerometer/point force, accelerometer/PZT actuator, PVDF sensor/point force, and PVDF sensor/PZT actuator can be derived as follows:

$$\alpha_{a_i f_j}(\omega)=\frac{x_{a_i}}{F_j}=\sum_{n=1}^{\infty}\frac{\phi_{ni}^{a}\phi_{nj}^{f}}{\rho_b b t_b[(\omega_n^2-\omega^2)+i(2\xi_n\omega_n\omega)]} \tag{16}$$

$$\alpha_{a_i c_j}(\omega)=\frac{x_{a_i}}{V_{c_j}}=\sum_{n=1}^{\infty}\frac{\phi_{ni}^{a}\phi_{nj}^{c}}{\rho_b b t_b[(\omega_n^2-\omega^2)+i(2\xi_n\omega_n\omega)]} \tag{17}$$

$$\alpha_{p_i f_j}(\omega)=\frac{V_{p_i}}{F_j}=\sum_{n=1}^{\infty}\frac{\phi_{ni}^{p}\phi_{nj}^{f}}{\rho_b b t_b[(\omega_n^2-\omega^2)+i(2\xi_n\omega_n\omega)]} \tag{18}$$

$$\alpha_{p_i c_j}(\omega)=\frac{V_{p_i}}{V_{c_j}}=\sum_{n=1}^{\infty}\frac{\phi_{ni}^{p}\phi_{nj}^{c}}{\rho_b b t_b[(\omega_n^2-\omega^2)+i(2\xi_n\omega_n\omega)]} \tag{19}$$

where

$$\phi_{ni}^{a}=\sqrt{\frac{2}{L}}\sin\kappa_n x_{a_i} \tag{20}$$

$$\phi_{nj}^{f}=\sqrt{\frac{2}{L}}\sin\kappa_n x_{f_j} \tag{21}$$

$$\phi_{ni}^{p}=K_p\kappa_n\sin(\kappa_n l_p/2)\sqrt{\frac{2}{L}}\sin\kappa_n x_{p_i} \tag{22}$$

$$\phi_{nj}^{c}=K_c\kappa_n\sin(\kappa_n l_c/2)\sqrt{\frac{2}{L}}\sin\kappa_n x_{c_j} \tag{23}$$

The response point is denoted by i, and the driving point is denoted by j. The subscripts and superscripts of a, f, p and c signify the accelerometer, point force, PVDF and PZT respectively. The numerator of FRFs which is know as "modal constant" (Ewins, 1986) is the product of two mode shape elements. Equations (20)-(23) neglecting subscripts i and j can be identified as the mode shapes of accelerometer, point force, PVDF sensor and PZT actuator respectively. One can easily demonstrate that those mode shapes are orthogonal to each others. In particular, ϕ_n^a and ϕ_n^f are orthonormal pairs. This implies that either pair of piezoceramic and conventional transducers as shown in Equations (16)-(19) can be used to perform structural modal testing. Once the frequency response function is measured, any suitable curve fitting algorithm can be applied to determine the modal parameters including natural frequencies, damping ratios and mode shapes. It is noted that the formulation is only valid for the conditions which the central location of distributed actuator and sensor coincides with the location of point actuator and sensor, i.e., $x_{a_i}=x_{p_i}$ and $x_{f_j}=x_{c_j}$.

The transfer functions between the i-th point (accelerometer) sensor and the i-th distributed (PVDF) sensor based on the j-th point force and the j-th PZT excitation can be defined as follow respectively:

$$\alpha_{a_i p_i/f_j}(\omega)=\frac{\alpha_{a_i f_j}(\omega)}{\alpha_{p_i f_j}(\omega)} \tag{24}$$

$$\alpha_{a_i p_i/c_j}(\omega)=\frac{\alpha_{a_i c_j}(\omega)}{\alpha_{p_i c_j}(\omega)} \tag{25}$$

The transfer functions between the j-th point force and the j-th distributed (PZT) actuator based on the i-th point (accelerometer) sensor and the i-th distributed (PVDF) sensor can be defined as follow respectively:

$$\alpha_{f_j c_j/a_i}(\omega)=\frac{\alpha_{a_i f_j}(\omega)}{\alpha_{a_i c_j}(\omega)} \tag{26}$$

$$\alpha_{f_j c_j/p_i}(\omega)=\frac{\alpha_{p_i f_j}(\omega)}{\alpha_{p_i c_j}(\omega)} \tag{27}$$

The block diagram is shown in Figure 2.

NUMERICAL RESULTS AND DISCUSSIONS

A steel beam with length of 0.38 m, width of 0.04 m, and thickness of 2 mm is used in the simulations. The natural frequencies are shown in Table 1. The beam is equally divided into 19 divisions as shown in Figure 1. The accelerometers and point forces are placed at the central location of each division, while the PVDF sensors and PZT actuators are sized with a length of 0.02 m and applied over a full division. The piezoelectric patch (G-1195) (Piezo Systems, 1990) and PVDF films (LDT-28$_\mu$k) (Pennwalt Corporation, 1990) are respectively used. Their physical properties are shown in Tables 2 and 3 respectively. The damping ratios are assumed to be 0.01 for all modes. In considering the convergence of series, 40 modes are included for

numerical simulation. In the following examples, the amplitude and phase angle of the point and transfer FRFs for i=2, j=2 and i=19, j=2 are shown and plotted over a frequency range of 10-10000 Hz in logarithmic scale.

The mode shapes of accelerometers, point force, PVDF sensor and PZT actuators are shown to have the same sinusoidal form for simply supported beam except exhibiting a different scale. The scaling values depends on the structural modal number and the length of PVDF sensor and PZT actuator as shown in Equations (20)-(23). The first five mode shapes of accelerometer and point forces represented by 19 points is shown in Figure 3.

Characteristics of Point FRF. Figures 4(a)-4(d) show the point FRFs between actuators/sensors for i=2 and j=2, i.e., the driving point coincides with the response point, corresponding to Equations (16)-(19). As expected, the resonant frequencies agree well for all FRFs, and the antiresonances appear right between resonances. The phase angle is also shown and denoted by the dotted line. One can observe that 90° phase angle changes at each resonance and antiresonance. The first point to notice is that α_{af} and α_{pf} have different antiresonance frequencies due to the sign change of modal constant which is the product of mode shape elements. Secondly, α_{af} reveal a mass-dominated characteristic which tends to drift downward, while α_{pc} shows a stiffness-dominated behavior and tends to drift upward. Finally, at lower frequencies α_{pc} exhibits relatively small peak at resonances.

In order to further compare the FRFs, all FRFs are scaled based on the values of α_{af} at 10 Hz and plotted in Figure 5. It is noted that α_{ac} and α_{pf} coincides exactly. This can be explained by the comparison of Equations (17) and (18) in which the modal constants for both FRFs are proportional to each others. α_{af} provides lower gains than α_{pf} at high frequencies, and α_{pf} provides more gain than α_{pc}. This result contradicts to that by (Collins et al., 1991). They showed that the gain of distributed (PVDF) sensor is lower than that of point (accelerometer) sensor at higher frequencies, when the point force excitation is applied.

Figures 6(a) and 6(b) show the transfer function between accelerometer and PVDF sensor based on the point force excitation and PZT excitation corresponding to Equations (24) and (25) respectively. Both $\alpha_{ap|f}$ and $\alpha_{ap|c}$ reveal resonances and antiresonances. The resonances of $\alpha_{ap|f}$ are right at the antiresonances of α_{pf}, and the antiresonances are at the antiresonances of α_{af}. This can be clearly understood from the FRF equation shown previously. There is phase change at resonance and antiresonance as discussed before. Similar characteristics can be found for $\alpha_{ap|c}$. It is interested to note that $\alpha_{ap|f}$ and $\alpha_{ap|c}$ reveal quite different resonances and antiresonances, and $\alpha_{ap|f}$ is generally higher than $\alpha_{ap|c}$. This means that PZT actuators can provide more gain than point force actuators in conjunction with the use of either PVDF or accelerometers. It is also noticed that the shapes of $\alpha_{fc|a}$ and $\alpha_{fc|p}$ as shown in Figures 6(c) and (d) match exactly with $\alpha_{ap|f}$ and $\alpha_{ap|c}$ respectively and just have a different scale. This implies that PVDF can provide more gain than accelerometers.

Characteristics of Transfer FRF. Figures 7-9 show the FRFs corresponding to Figures 4-6 except that i=19 and j=2, i.e., the driving point is far away from the response point. This is so called the transfer FRF. Similar observations can be made as those discussed in point FRFs. The main differences are that there are no antiresonances between resonances, and the phase

change may cross over 0° or 180° at the lobe frequencies in Figure 7. Again, α_{af} reveal a mass-dominated characteristic, while α_{pc} shows a stiffness-dominated behavior. Figure 8 again shows all FRFs which are scaled based on the values of α_{af} at 10 Hz. One can observe that the point actuator/sensor can provide more gain the distributed ones all over the specified frequencies range. Figure 9(a) and 9(b) show the FRFs of α_{aplf} and α_{aplc} defined in Equations (24) and (25). One can observe that both FRFs match very well except those frequencies below 30 Hz. This means that when driving point and response point are far away enough, both accelerometer and PVDF sensors result in the same effect for either point or distributed excitation. Also, at higher frequencies the PVDF sensors provide relatively more gains than the accelerometers.

CONCLUSIONS

This paper characterizes the transfer functions between point/distributed actuators and point/distributed sensors. Four pairs of sensors and actuators, such as accelerometer/point force, accelerometer/PZT, PVDF/point force and PVDF/PZT, are investigated. The FRFs are derived and expressed in the modal model format. The individual mode shape is also identified and shown its orthogonality for the conditions which the central location of distributed actuator/sensor is coincident with that of point actuator/sensor. This implies that the distributed actuator/sensor can be utilized for structural modal testing. The modal parameters including natural frequencies, mode shapes and damping ratios can be obtained by any suitable curve-fitting algorithm, once the FRFs are available. Additionally, the characteristic of point and transfer FRFs are studied. Results show that the distributed actuator/sensor can generally provide more gain than the point actuator/sensor. This work not only draws an ideas for applications of smart structural testing to system identification and diagnosis but also compares the transfer functions between piezoceramic and conventional transducers leading to active control applications.

REFERENCES

Alberts, T. E. and Colvin, J. A., "Observations on the Nature of Transfer Functions for Control of Piezoelectric Laminates," *Journal of Intelligent Material Systems and Structures*, Vol. 2, pp. 528-541 (1991).

Clark, R. L., Fuller, C. R., and Wicks, A., "Characterization of Multiple Piezoelectric Actuators for Structural Excitation," *Journal of Acoustical Society of America*, Vol. 90, pp. 346-357 (1991).

Collins, S. A., Miller, D. W., and von Flotow, A. H., "Piezopolymer Spatial Filters for Active Structural Control," *Proceedings of the Conference on Recent Advances in Active Control of Sound and Vibration*, pp. 219-234 (1991).

Crawley, E. F. and de Luis, J., "Use of Piezoelectric Actuators as Elements of Intelligent Structures," *AIAA Journal*, Vol. 25, pp. 1373-1385 (1987).

Dimitriadis, E. K., Fuller, C. R., and Rogers, C. A., "Piezoelectric Actuators for Distributed Vibration Excitation of Thin Plate," *Journal of Vibration and Acoustics*, Vol. 113, pp. 100-107 (1991).

Ewins, D.J., *Modal Testing: Theory and Practice*, Research Studies Press Ltd., Letchworth, Hertfordshire, England, (1986).

Hubbard, J. E., "Distributed Sensors and Actuators for Vibration Control in Elastic Components," *Noise-Con 87*, pp. 407-412 (1987).

Im, S. and Atluri, S. N., "Effects of a Piezo-Actuator on a Finitely Deformed Beam Subjected to General Loading," *AIAA Journal*, Vol. 27, pp. 1801-1807 (1989).

Lee, C. K. and Moon, F. C., "Modal Sensors/Actuators," *Journal of Applied Mechanics*, Vol. 57, pp. 434-441 (1990).

Pennwalt Corporation, , *Piezo Film Sensor Application Notes*, (1990).

Piezo Systems, Inc., *Product Catalog*, (1990).

Sun, F. P., Liang, C., and Rogers, C. A., "Experimental Modal Testing Using Piezoceramic Patches as Collocated Sensor-Actuators," *Proceedings of the 1994 SEM Spring Conference and Exhibits*, pp. 871-879 (1994).

Wang, B. T. and Rogers, C. A., "Modeling of Finite-Length Spatially Distributed Induced Strain Actuators for Laminate Beams Structures," *Journal of Intelligent Material Systems and Structures*, Vol. 2, pp. 38-58 (1991).

Table 1. Natural frequencies of the simply-supported beam

mode	frequency (Hz)	mode	frequency (Hz)
1	33.2	6	1159.6
2	128.8	7	1578.3
3	289.9	8	2061.4
4	515.4	9	2609.0
5	805.3	10	3220.9

Table 2. Physical properties of the G-1195 piezoceramic patch (Piezo Systems, 1990)

E_a-6.3×10^{10}(N/m^2)	ρ_a-7650 (Kg/m^3)
t_a-1.905(mm)	ν_a-0.28
d_{31}-d_{32}-166×10^{-12}($\frac{m}{volt}$)	

Table 3. Physical properties of the PVDF films (LDT-28$_\mu$k) (Pennwalt Corporation, 1990)

E_p-2×10^9(N/m^2)	ρ_p-1800 (Kg/m^3)
t_p-28×10^{-6}(m)	ν_p-0.33
e_{31}-54×10^{-3}(C/m)	ϵ-106×10^{-12}(F/m)

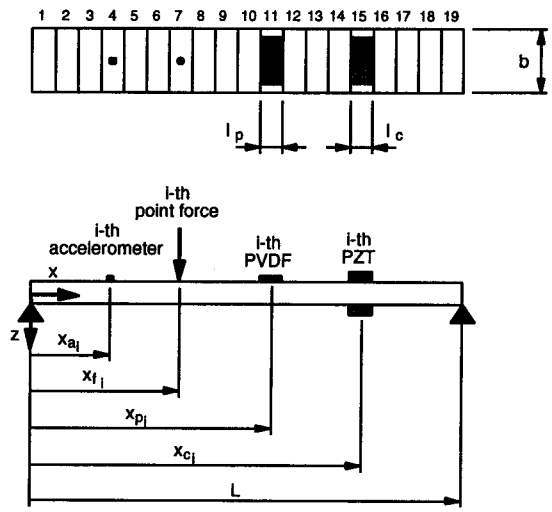

Figure 1. The arrangement and coordinates of simply-supported beam

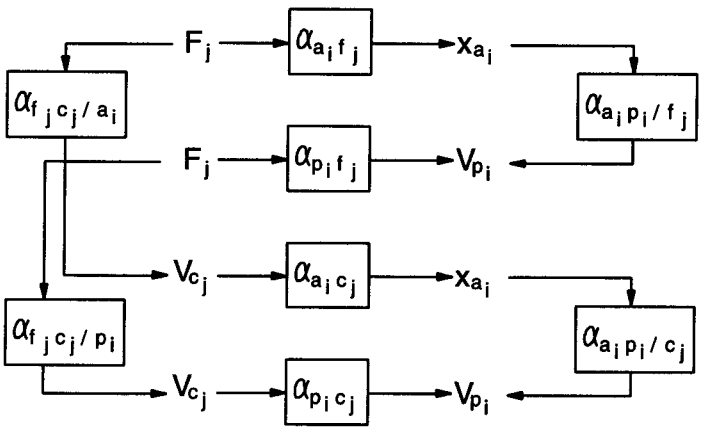

Figure 2. Block diagram of frequency response function

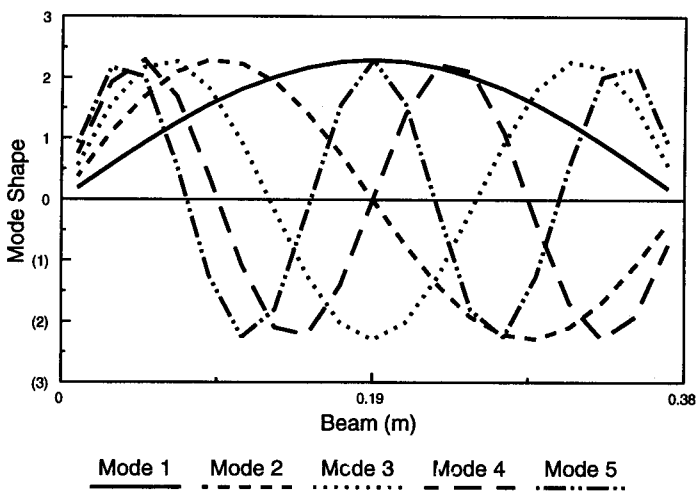

Figure 3. Mode shapes for accelerometer and point force

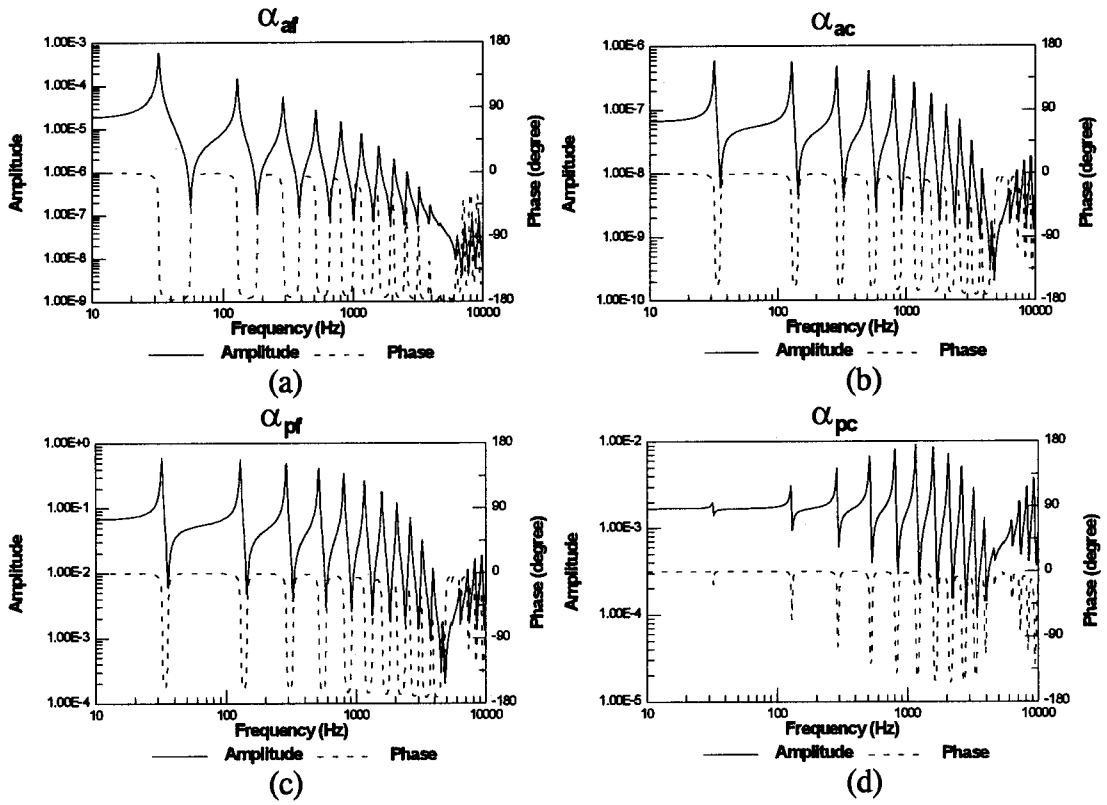

Figure 4. Point FRF between actuator/sensor for i=2, j=2

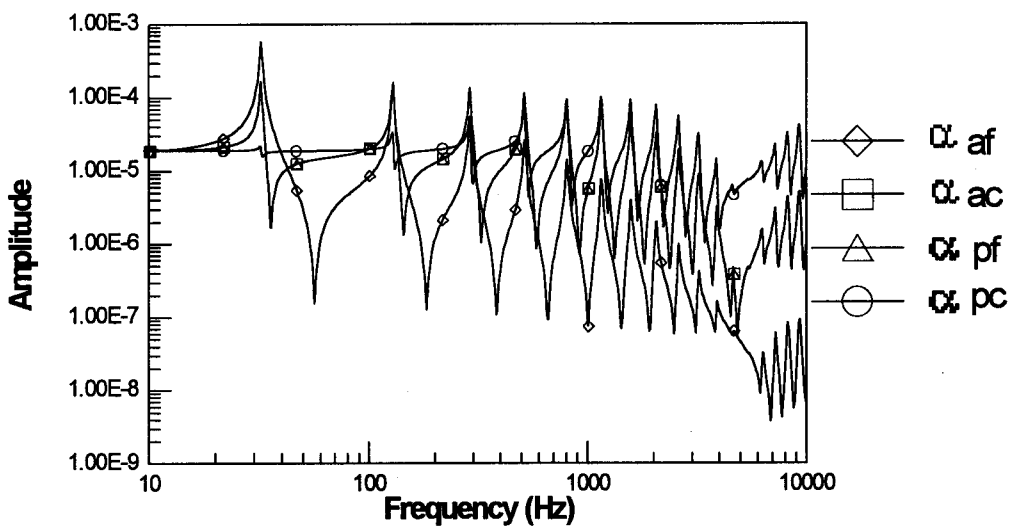

Figure 5. Comparison of point FRFs between actutor/sensor for i=2,j=2

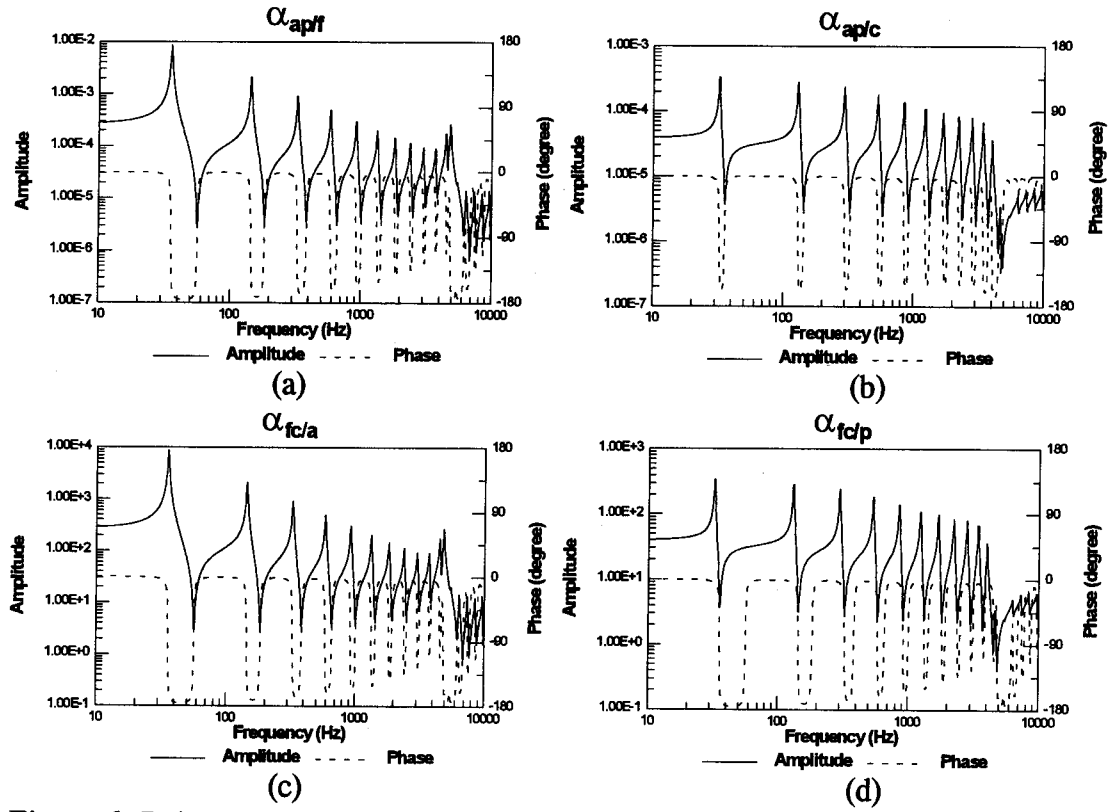

Figure 6. Point FRF of point/distributed actuator/sensor for i=2,j=2

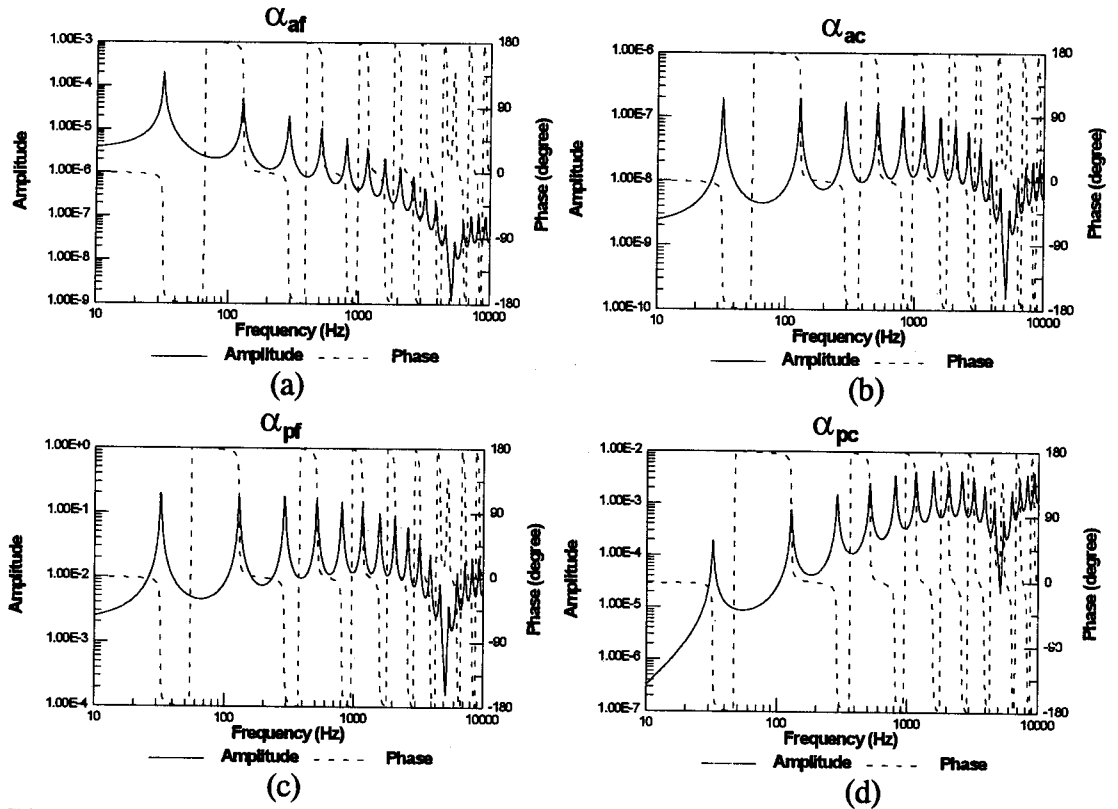

Figure 7. Transfer FRF between actuator/sensor for i=19, j=2

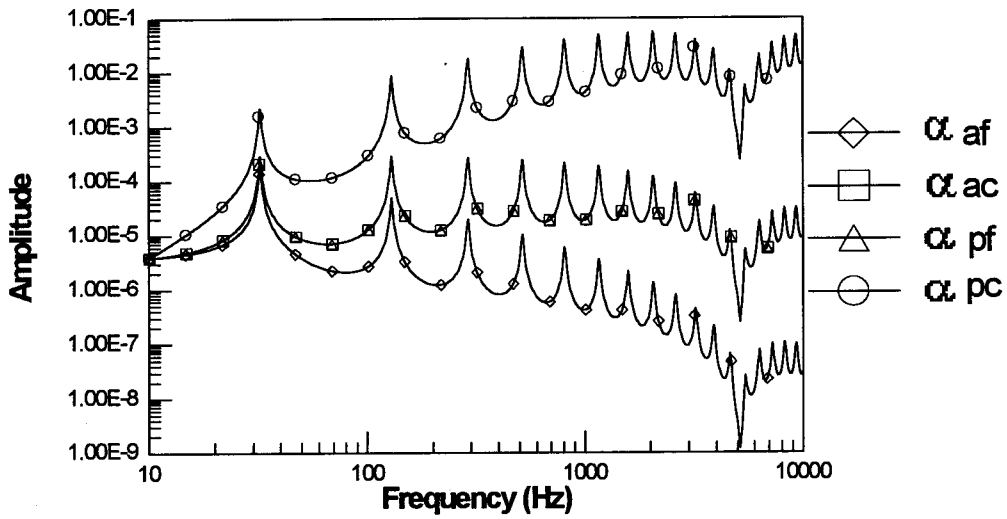

Figure 8. Comparison of transfer FRF between actuator/sensor for i=19, j=2

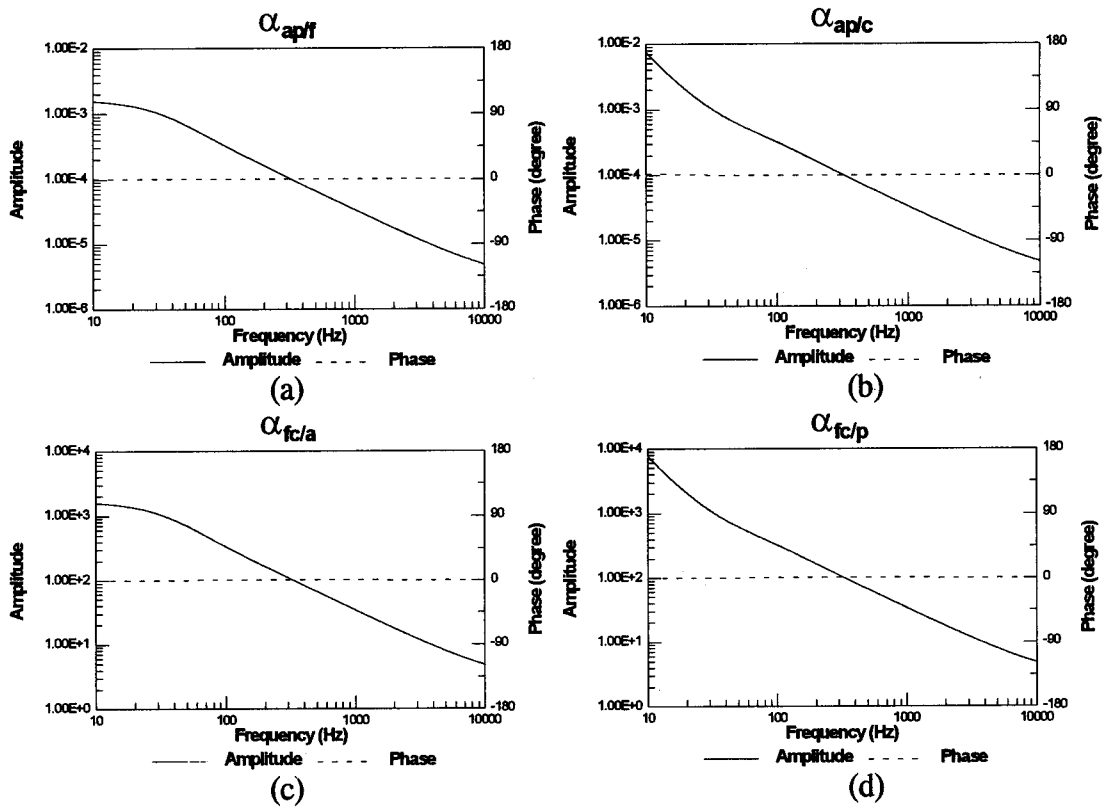

Figure 9. Transfer FRF of point/distributed actuator/sensor for i=19,j=2